DE GRUYTER
OPEN

Study on the effect of atmospheric gases adsorbed in MnFe₂O₄/MCM-4l nanocomposite on *ortho*-positronium annihilation

**Marek Wiertel,
Zbigniew Surowiec,
Mieczysław Budzyński,
Wojciech Gac**

Abstract. In this paper, results of positron annihilation lifetime spectroscopy (PALS) studies of MnFe₂O₄/MCM--41 nanocomposites in N_2 and O_2 atmosphere have been presented. In particular, the influence of manganese ferrite loading and gas filling on *pick-off ortho*-positronium (*o*-Ps) annihilation processes in the investigated samples was a point of interest. Disappearance of the longest-lived *o*-Ps component with τ_5 present in the PAL spectrum of initial MCM-41 mesoporous material in the PAL spectra of MnFe₂O₄-impregnated MCM-41 measured in vacuum is a result of either a strong chemical *o*-Ps quenching or the Ps inhibition effects. The intensity I_4 of the medium-lived component initially increases, reaching a maximum value for the sample with minimum manganese ferrite content, and then decreases monotonically. Analogous dependence for the intensity I_3 of the shortest-lived component shows a maximum at higher MnFe₂O₄ content. Filling of open pores present in the studied nanocomposites by N_2 or O_2 at ambient pressure causes partial reappearance of the τ_4 and τ_5 components, except a sample with maximum ferrite content. The lifetimes of these components measured in O_2 are shortened in comparison to that observed in N_2 because of paramagnetic quenching. Anti-inhibition and anti-quenching effects of atmospheric gases observed in the MnFe₂O₄/MCM-41 samples are a result of neutralization of some surface active centers acting as inhibitors and weakening of *pick-off* annihilation mechanism, respectively.

Key words: manganese ferrite • MCM-41 silica • nanocomposite • *o*-Ps quenching • positronium annihilation

M. Wiertel✉, Z. Surowiec, M. Budzyński
Department of Nuclear Methods,
Institute of Physics,
M. Curie-Skłodowska University,
1 M. Curie-Skłodowskiej Sq., 20-031 Lublin, Poland,
Tel.: +48 81 537 6220, Fax: +48 537 6191,
E-mail: marek.wiertel@umcs.lublin.pl

W. Gac
Faculty of Chemistry,
M. Curie-Skłodowska University,
3 M. Curie-Skłodowskiej Sq., 20-031 Lublin, Poland

Introduction

A nanocomposite is a multiphase solid material in which one of the phases has one, two, or three dimensions of less than 100 nm or structures having nanoscale repeat distances between the different phases that make up the material [1]. The mechanical, electrical, thermal, optical, electrochemical, and catalytic properties of the nanocomposite will differ markedly from that of component materials. Regarding synthesis route and a purpose of fabrication, a nanocomposite may be treated as a matrix to which nanoparticles have been added to improve or change a particular property of the material. Nanocomposites are attractive researching subject from both practical and theoretical point of view because of the possibility to get nanomaterials with determined functionality.

In the practical applications, the knowledge of porosity of nanocomposites is of primary importance. The PALS technique is one of the very promising methods used for its study [2]. Among other parameters, this method allows to determine the diameters of pore and other free spaces using the Tao-Eldrup model [3, 4] and its extensions [2]. These models are based on the fact that the intrinsic

lifetime of *ortho*-positronium (*o*-Ps) is reduced from 142 ns in vacuum by the process called *pick-off* annihilation. Hence, the *o*-Ps lifetime is dependent on the size of the pore in which the *o*-Ps atom is trapped. This gives a possibility to use *o*-Ps as a porosimetric probe to evaluate the average sizes in the approximate range from a few tenths of nanometer to 100 nm. A complete or partial filling of the pores by some chemical species is a source of occurrence of various processes to which *o*-Ps living in localized states long enough is subject. The examples of such phenomena are chemical reactions and scattering on paramagnetic molecules associated with spin--flop transition. As a result of those processes, the *pick-off* lifetime of *o*-Ps may be further shortened. Relevant processes are called chemical quenching and paramagnetic quenching (or *ortho-para* conversion), respectively [5]. Chemical reactions with the so-called inhibitors, in turn, lead to inhibition of Ps formation and only have an effect on values of *o*-Ps lifetime components intensities. Chemically active centers scavenging electrons, positrons, holes, and so on also act as inhibitors. All phenomena enumerated above may potentially give valuable information on the structural and chemical properties of micro- and mesoporous materials, on the one hand, and they may make obtaining quantitative results on pore sizes hard or even impossible, on the other hand.

Also, attempts have been made to create a model using a positron component, which could be applicable when *o*-Ps is not formed in available free volumes [6].

A lot of efforts so far have been made in order to properly take into account the effects of pore surface chemistry, gas filling [7] on relation between pore sizes, and *o*-Ps lifetimes.

Highly ordered mesoporous MCM-41 silica can be used as a support for magnetic ferrite nanoparticles or, after being modified, as a support for putting of specific chemical functional groups. It is characterized by uniform pore diameter distribution, large total pore volume, and large specific surface area [8]. Free-volume structure in them is represented by primary pores along with specific vacancy-type defects within individual crystalline grains and intergranular boundaries.

The aim of presented investigations was to give more details concerning the influence of gaseous N_2 and O_2 adsorbed in $MnFe_2O_4$/MCM-41 nanocomposites on mean lifetime of *o*-Ps. Additionally, possibility to use PALS method for the quantitative or semi--quantitative characterization of internal structure of such materials in the microscale is examined.

Experimental

The samples of $MnFe_2O_4$/MCM-41 nanocomposites with nominal Fe content equals to 5, 10, 20, and 40 wt% at constant molar relation Fe/Mn as 2:1 were obtained in two stages. First, the high surface mesoporous MCM-41 support was prepared. Next the appropriate portions of Fe and Mn from iron nitrate $Fe(NO_3)_3 \times 9H_2O$ and manganese acetate $Mn(CH_3COO)_2 \times 4H_2O$ ethanol solutions were embedded into silica support by means of an incipient wetness impregnation method. The samples were initially dried at 100°C and next calcined at 400°C for 3 h. The relatively low-calcination temperature has been dictated by intention to obtain as small as possible ferrite particles dimensions with maximum dispersion in the support. Next the samples were examined by XRF (X-ray fluorescence) method. From XRF results, actual Fe and Mn contents were obtained. Their values are equal to 4.3, 8.6, 17.2, and 35.2 for Fe wt%, 2.2, 4.3, 8.9, and 17.9 for Mn wt% and for the samples denoted in this paper by A, B, C, and D, respectively.

The investigations regarding the surface morphology for the investigated samples have been made using two techniques: scanning electron microscopy (SEM) and transmission electron microscopy (TEM). The apparatus used for SEM characterization is a Tescan Vega3 LMU microscope using secondary electrons as signal with the acceleration voltage of 30 kV. For microstructure characterization, we have used a TEM FEI Tecnai G2 20 X-TWIN.

In PALS measurements, the ^{22}Na positron source sealed in a Kapton envelope (8 μm thick) sandwiched between two identical sample pellets of about 2 mm thick was used. This assembly was put in the vacuum chamber equipped with a gas handling system to admit high-purity nitrogen (N 5.0, BOC Gazy) and oxygen (O 4.5, Air Products). The used turbomolecular pump allows us to obtain vacuum of the order of 5×10^{-4} Pa. Positron lifetime spectra were recorded at room temperature using a standard fast-slow coincidence spectrometer with pulse pile-up inspection. The spectrometer was equipped with two scintillation counters consist of cylindrical BaF_2 coupled to XP2020Q photomultiplier tubes. The geometry excluding the possibility of summing effects was used [9]. Because of, in porous media, a substantial number of *o*-Ps atoms annihilates intrinsically into 3γ-quanta mode, energy spectrum in such annihilation mode is continuous, extending from 0 to 511 keV. Thus, to improve the efficiency of counting, the stop energy window in the spectrometer was widely open (80% of the energy range). At such a setting, the resolution time was 270 ps (measured for ^{60}Co source with ^{22}Na windows set). The time base of the PALS setup was 1 μs (8192 channels). The total counts were not less than 10^8 for each spectrum measured in vacuum or in air. Before starting measurement in vacuum, each sample was outgassed at 200°C for 8 h. In order to avoid the influence of dynamic effects associated with gas filling processes [10] on PALS results, the spectra were started to measure after about 120 h from the moment of filling up the sample chamber with gas. After that time interval, all annihilation parameters were stabilized what was checked by observing 3-h spectra time evolution.

The positron lifetime spectra were analyzed using the LT9 program [11]. A source component 0.382 ns (annihilation in Kapton foil) of intensity in the range of about (11÷13)% was taken into account in lifetime data processing.
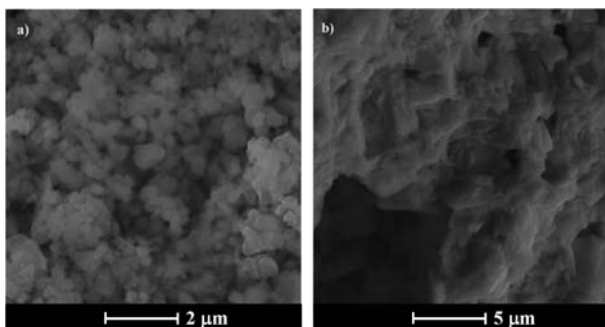
**Fig. 1.** The SEM images of the mesoporous silica: (a) empty MCM-41 and (b) MnFe$_2$O$_4$/MCM-41 (B).

Results and discussion

The porous structure and surface properties of the MCM-41 matrix change significantly after incorporation of MnFe$_2$O$_4$ into this mesoporous support. Manganese ferrite takes the form of nanoparticles and output material forms nanocomposite. The SEM images of the mesoporous MCM-41 silica obtained for empty template and sample MnFe$_2$O$_4$/MCM-41 (B) are presented in Fig. 1. The sample with pure MCM-41 silica (Fig. 1a) shows a more granular form in comparison with the impregnated MCM-41 sample (Fig. 1b). The first sample shows a well-defined spherical morphology with small agglomerates with sizes between 300 and 500 nm, whereas the other sample exhibits more compact and smoother morphology of surface with bigger non-spherical particles. The microstructure of the obtained samples is clearly revealed by TEM. Figure 2 shows the images for the low- and high-loaded MnFe$_2$O$_4$/MCM-41 silica. Once again the MCM-41 support with low content of MnFe$_2$O$_4$ (Fig. 2a) shows spherical shape with a highly ordered hexagonal long-range array of the channels. TEM image of MnFe$_2$O$_4$/MCM-41 (D) sample (Fig. 2b) shows that the mesoporous structure is preserved and the nanocrystallites of manganese ferrite are located in nanochannels of MCM-41 silica. The length of nanochannels observed at TEM images is in the same range as a size of particles that are visible on the SEM images.

In Fig. 3, five different PAL spectra for investigated samples measured in O$_2$ atmosphere (bottom panel) and in N$_2$ at ambient pressure (top panel) are presented. All the spectra can be well decom-
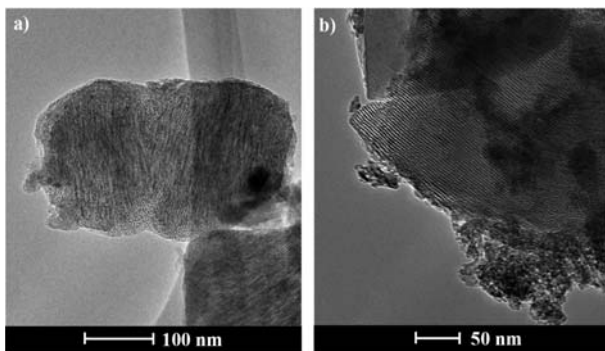
Fig. 2. The TEM images of the nanocomposite samples: (a) MnFe$_2$O$_4$/MCM-41 (B) and (b) MnFe$_2$O$_4$/MCM-41 (D).
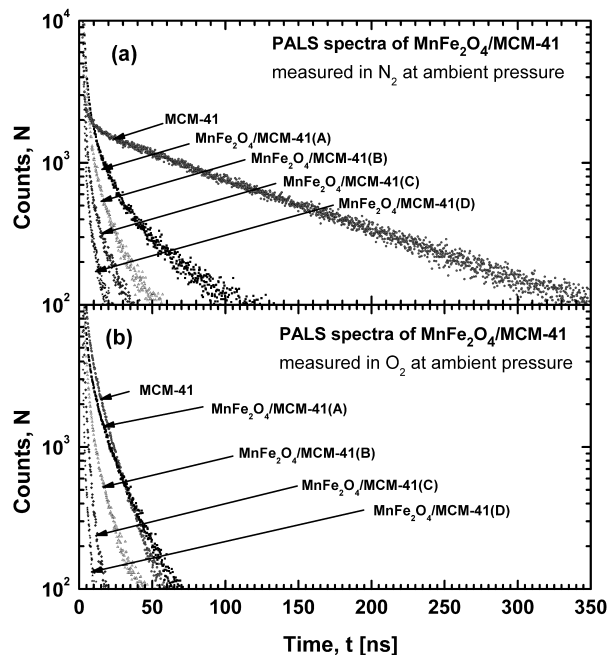
Fig. 3. Positron annihilation lifetime spectra of empty MCM-41 and four MnFe$_2$O$_4$/MCM-41 samples measured in N$_2$ (upper) and O$_2$ (below) under 10^5 Pa pressure, normalized to time of measurement. Background is subtracted.

posed into five discrete exponential components. The first two are relatively short-lived. The former belongs in principle to the intrinsic decay of *para*-positronium (*p*-Ps, $\tau_1 \approx 0.13$ ns) and the latter is related to the free annihilation of positrons trapped at defects located in the amorphous silica walls [12] or in vacancy clusters existing in the bulk of ferrite nanoparticles [13] or on their surfaces [14]. The observed value of $\tau_2 \approx 0.45$ ns is an average value for two above-mentioned groups of positrons. The τ_1 parameter was fixed in the fitting procedure in order to obtain acceptable standard uncertainties for the parameters of long-lived *o*-Ps components. The second component's lifetime value τ_2 remains almost constant but its intensity changes from about 39% in pure MCM-41 to about 90% in the sample (D) very similar for all series of measurements in vacuum, in O$_2$ and N$_2$. It is simply related to the increasing amount of manganese ferrite nanoparticles deposited mainly on surfaces of MCM-41 walls.

In contrary to the PALS results in nanocrystalline ferrites prepared by other method [15], in MnFe$_2$O$_4$/MCM-41 nanocomposite, a bulk lifetime component of about 0.2 ns is not observed. From PALS analysis, the lifetime and intensity relating to positron free annihilation in the non-defective nanocrystalline grain volumes were derived for analogous NiFe$_2$O$_4$(SiO$_2$) composite obtained by sol-gel method [16, 17]. The lifetime, denoted by authors as τ_n, is equal to about 0.14 ns. In the samples investigated by us, MnFe$_2$O$_4$/MCM-41 nanocomposite a component of lifetime in the same range was not found. One can conclude that in the manganese ferrite, nanocomposite samples obtained by the wetness impregnation route are defective in almost all volume.

In the investigated samples three long-lived *o*-Ps components were also observed in the positron

Table 1. The lifetimes and intensities of *o*-Ps components measured in vacuum ($p \approx 5 \times 10^{-4}$ Pa), N_2 and O_2 for ferrite $MnFe_2O_4$/MCM-41 nanocomposite samples. The results for measurements in vacuum are taken from [18]

| Sample		τ_3	τ_4	τ_5	I_3	I_4	I_5
		[ns]			[%]		
Empty MCM-41	vacuum	3.46(38)	33.1(2.0)	124.92(80)	1.07(16)	0.88(33)	23.40(40)
	N_2	0.97(22)	27.1(1.7)	124.41(71)	3.25(59)	0.72(25)	22.51(38)
	O_2	1.76(23)	6.95(49)	16.94(53)	11.97(57)	7.63(41)	6.28(51)
$MnFe_2O_4$/MCM-41(A) 4.3 wt% Fe	vacuum	2.00(23)	10.54(51)	40.46(87)	6.01(44)	3.27(22)	2.50(24)
	N_2	1.97(18)	12.57(43)	69.37(83)	6.03(37)	3.42(23)	3.91(25)
	O_2	1.95(28)	8.02(55)	23.52(57)	7.33(54)	4.38(31)	4.94(36)
$MnFe_2O_4$/MCM-41(B) 8.6 wt% Fe	vacuum	1.56(18)	7.30(54)	26.95(87)	9.90(53)	1.98(21)	1.38(23)
	N_2	1.66(14)	9.75(44)	48.40(1.0)	9.12(47)	2.31(22)	1.41(19)
	O_2	1.72(22)	6.49(53)	20.98(79)	7.85(49)	2.61(26)	1.43(27)
$MnFe_2O_4$/MCM-41(C) 17.2 wt% Fe	vacuum	1.49(29)	6.74(79)	26.60(1.1)	4.11(56)	1.08(18)	0.92(24)
	N_2	1.47(25)	6.98(61)	28.29(95)	4.17(50)	1.18(19)	0.95(20)
	O_2	1.52(67)	4.81(21)	14.80(1.7)	1.22(30)	1.50(1.4)	0.20(27)
$MnFe_2O_4$/MCM-41(D) 35.2 wt% Fe	vacuum	1.73(33)	7.14(73)	29.3(2.2)	1.63(32)	0.77(19)	0.19(18)
	N_2	1.14(30)	6.14(64)	27.3(1.3)	2.85(73)	0.67(12)	0.38(16)
	O_2	1.43(51)	4.70(1.0)	15.6(2.2)	1.33(51)	0.52(29)	0.13(25)

lifetime spectra. Detailed values of their lifetimes and intensities are given in Table 1 and are presented in Fig. 4. For the comparison in this table, the lifetimes and intensities measured earlier [18] are also quoted. For pure MCM-41 sample under different atmospheres, the component with the lifetime τ_3 ranging from 3.5 to 1.5 ns arises owing to the *pick-off* annihilation of *o*-Ps formed in the some kind of open-volume defects on the surfaces of amorphous silica walls. In the nanocomposite samples, the lifetime of this component at first rapidly decreases for the sample $MnFe_2O_4$/MCM-41(A) and then diminishes only slightly as ferrite loading increases. The values of τ_3 are practically independent on the kind of gas filling sample. It suggests that this component

is related mainly to the defects of closed type. For measurements in N_2 atmosphere, I_3 increases by about three times and achieves a maximum in the sample $MnFe_2O_4$/MCM-41(B) in order to fall to about 3%. A course of I_3 dependence measured in O_2 is very similar but with lower values at higher ferrite contents and quite surprisingly much higher value for pure silica. It seems that a screening effect of silica surface coverage by O_2 is significantly stronger than a screening for ferrite surfaces.

The lifetimes from about 1.9 to 3.2 ns related to the *pick-off* annihilation of *o*-Ps atoms formed inside large voids for bulk nanocrystalline ferrites were observed in [13]. They are close to that in our measurements what can explain increase of I_3 with the increase of ferrite content.

The medium-lived component τ_4 results from decay of *o*-Ps trapped inside of silica nanochannels, and the longest-lived component τ_5 is related to the *pick-off* annihilation of *o*-Ps formed in free volumes in intergranular spaces of the material [19]. For the manganese ferrite composite samples, the lifetime τ_4 is reduced by factor of three. Accordingly to our interpretation of these components origin, these characters of dependences indicate that inner spaces (pores) volumes lessen owing to filling with ferrite. In contrast to Fe-modified MCM-41 silica [20], in which Fe is incorporated into silica walls in the stage of MCM-41 making, also the τ_5 lifetime for the manganese ferrite nanocomposite considerably decreases. Generally, the intensities I_4 and I_5 decrease with increasing ferrite content, but simultaneously, their values obtained for the nanocomposite samples measured at N_2 or O_2 atmosphere samples are slightly bigger in comparison to those observed in vacuum. It is right only for samples with ferrite content of up to about 9% what indicates both the inhibition and quenching phenomena occur.

The difference between PAL spectra measured in O_2 and N_2 manifesting as considerable larger intensity of the longest-lived component in the latter
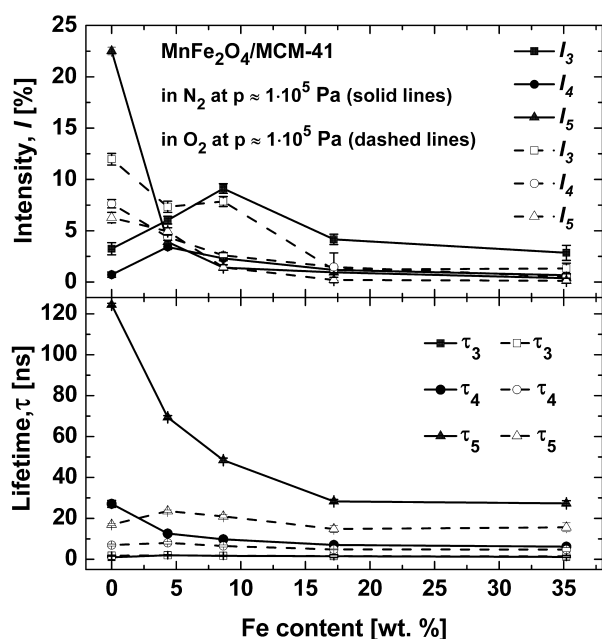
Fig. 4. The dependences of lifetimes (lower panel) and intensities (upper panel) of the three *o*-Ps components on Fe content for the $MnFe_2O_4$/MCM-41 nanocomposites measured in N_2 and O_2 at atmospheric pressure.

medium is caused mainly by *ortho-para* conversion occurring only for oxygen. However, it seems that the differences in chemical interaction and screening effect because of the blocking of active sites on the pore surface for the both used atmospheric gases may play a certain role [21]. Moreover, it is possible to observe long-lived components in positron lifetime spectra even by using strongly quenching *o*-Ps gas, which is oxygen.

Conclusions

The use of PALS method in a direct way to determine the pore sizes in complex material such as nanocomposites containing components with high electron densities is impossible using currently existing models. An interpretation of results is made difficult because of strong influence on disturbing factors such as chemical quenching and inhibition on parameters of long-lived components. The chemical quenching effect and also inhibition of the *o*-Ps formation must be prevented or at least weakened by an adsorption of gas chosen to a specific sample. This could allow one to use the positron annihilation parameters in investigation of its porosity. In order to use PALS technique for obtaining quantitative results in composite materials development of new model is needed, which would take into account not only the size of pores but also the quenching processes and the inhibition of Ps formation.

References

1. Ajayan, P. M. (2003). Bulk metal and ceramics nanocomposites. In P. M. Ajayan, L. S. Schadler, & P. V. Braun (Eds.), *Nanocomposite science and technology* (pp. 1–76). Weinheim: Wiley-VCH Verlag GmbH & Co. KgaA.
2. Goworek, T. (2014). Positronium as a probe of small free volumes in crystals, polymers and porous media. *Ann. UMCS Chemia*, *69*(1/2), 1–110. DOI: 10.2478/umcschem-2013-0012.
3. Tao, S. J. (1972). Positronium annihilation in molecular substances. *J. Chem. Phys.*, *56*, 5499–5510. DOI: 10.1063/1.1677067.
4. Eldrup, M., Lightbody, D., & Sherwood, J. N. (1981). The temperature dependence of positron lifetimes in solid pivalic acid. *Chem. Phys.*, *63*, 51–58. DOI: 10.1016/0301-0104(81)80307-2.
5. Schrader, D. M., & Jean, Y. C. (1988). Introduction. In D. M. Schrader, & Y. C. Jean (Eds.), *Positron and positronium chemistry* (pp. 1–26). Amsterdam: Elsevier.
6. Kuo-Sung, L., Hongmin, Ch., Somia, A., Jen-Pwu, Y., Wei-Song, H., Kuier-Rarn, L., Juin-Yih, L., Chien-Chieh, H., & Jean, Y. C. (2011). Determination of free-volume properties in polymers without orthopositronium components in positron annihilation lifetime spectroscopy. *Macromolecules*, *44*, 6818–6826. DOI: 10.1021/ma201324k.
7. Zaleski, R., Dolecki, W., Kierys, A., & Goworek, J. (2012). n-Heptane adsorption and desorption on porous silica observed by positron annihilation lifetime spectroscopy. *Microporous Mesoporous Mater.*, *154*, 142–147. DOI: 10.1016/j.micromeso.2011.08.032.
8. Beck, J. S., Vartuli, J. C., Roth, W. J., Leonowicz, M. E., Kresge, C. T., Schmitt, K. D., Chu, C. T. W., Olson, D. H., Sheppard, E. W., McCullen, S. B., Higgins, J. B., & Schlenker, J. L. (1992). A new family of mesoporous molecular sieves prepared with liquid crystal templates. *J. Am. Chem. Soc.*, *114*(27), 10834–10843. DOI: 10.1021/ja00053a020.
9. Goworek, T., Górniak, W., & Wawryszczuk, J. (1992). The sources of distortions and errors in the analysis of positron lifetime spectra. *Nucl. Instrum. Methods Phys. Res. Sect. A-Accel. Spectrom. Dect. Assoc. Equip.*, *321*, 560–570. DOI: 10.1016/0168-9002(92)90068-F.
10. Surowiec, Z., Wiertel, M., Zaleski, R., Budzyński, M., & Goworek, J. (2010). Positron annihilation study of iron oxide nanoparticles in mesoporous silica MCM-41 template. *Nukleonika*, *55*(1), 91–96.
11. Kansy, J. (1996). Microcomputer program for analysis of positron annihilation lifetime spectra. *Nucl. Instrum. Methods Phys. Res. Sect. A-Accel. Spectrom. Dect. Assoc. Equip.*, *374*, 235–244. DOI: 10.1016/0168-9002(96)00075-7.
12. Dannefaer, S., Bretagnon, T., & Kerr, D. (1993). Vacancy-type defects in crystalline and amorphous SiO$_2$. *J. Appl. Phys.*, *74*(2), 884–890. DOI: 10.1063/1.354882.
13. Hassan, H. E., Sharshar, T., Hessien, M. M., & Hemeda, O. M. (2013). Effect of γ-rays irradiation on Mn-Ni ferrites: Structure, magnetic properties and positron annihilation studies. *Nucl. Instrum. Methods Phys. Res. Sect. B-Beam Interact. Mater. Atoms*, *304*, 72–79. DOI: 10.1016/j.nimb.2013.03.053.
14. Chakrabarti, S., Chaudhuri, S., & Nambissan, P. M. G. (2005). Positron annihilation lifetime changes across the structural phase transition in nanocrystalline Fe$_2$O$_3$. *Phys. Rev. B*, *71*, 064105. DOI: 10.1103/PhysRevB.71.064105.
15. Bandyopadhyay, S., Roy, A., Das, D., Ghugre, S. S., & Ghose, J. (2003). Investigation of nanocrystalline CoFe$_2$O$_4$ by positron annihilation lifetime spectroscopy. *Philos. Mag.*, *83*, 765–773. DOI: 10.1080/0141861021000042271.
16. Mitra, S., Mandal, K., Sinha, S., Nambissan, P. M. G., & Kumar, S. (2006). Size and temperature dependent cationic redistribution in NiFe$_2$O$_4$(SiO$_2$) nanocomposites: positron annihilation and Mössbauer studies. *J. Phys. D-Appl. Phys.*, *39*, 4228–4235. DOI: 10.1088/0022-3727/39/19/016.
17. Chakraverty, S., Mitra, S., Mandal, K., Nambissan, P. M. G., & Chattopadhyay, S. (2005). Positron annihilation studies of some anomalous features of NiFe$_2$O$_4$ nanocrystals grown in SiO$_2$. *Phys. Rev. B*, *71*, 024115. DOI: 10.1103/PhysRevB.71.024115.
18. Wiertel, M., Surowiec, Z., Gac, W., & Budzyński, M. (2014). Positron annihilation in MnFe$_2$O$_4$/MCM-41 nanocomposite. *Acta Phys. Pol. A*, *125*, 793–797. DOI: 10.12693/APhysPolA.125.793.
19. Kobayashi, Y., Ito, K., Oka, T., & Hirata, K. (2007). Positronium chemistry in porous materials. *Radiat. Phys. Chem.*, *76*, 224–230. DOI: 10.1016/j.radphyschem.2006.03.042.
20. Wiertel, M., Surowiec, Z., Budzyński, M., & Gac, W. (2013). Positron annihilation studies of mesoporous iron modified MCM-41 silica. *Nukleonika*, *58*, 245–250.
21. Chuang, S. Y., & Tao, S. J. (1971). Study of various properties of silica gel by positron annihilation. *J. Chem. Phys.*, *54*, 4902–4907. DOI: 10.1063/1.1674769.